Analysis of riverine suspended particulate matter fluxes (Gulf of Lion, Mediterranean Sea) using a synergy of ocean color observations with a 3-D hydrodynamic sediment transport model

Vincent Le Fouest, Malik Chami, Romaric Verney

AGU PUBLICATIONS

JGR

Journal of Geophysical Research: Oceans

RESEARCH ARTICLE

10.1002/2014JC010098

Key Points:
- Initialization of a 3-D hydrosedimentary model with ocean color satellite data
- Synergy improves land-ocean particulate fluxes model predictions by 48%
- Particulate size and sinking rate are key parameters during pulsed exports

Correspondence to:
V. Le Fouest,
vincent.le_fouest@univ-lr.fr

Citation:
Le Fouest, V., M. Chami, and R. Verney (2015), Analysis of riverine suspended particulate matter fluxes (Gulf of Lion, Mediterranean Sea) using a synergy of ocean color observations with a 3-D hydrodynamic sediment transport model, *J. Geophys. Res. Oceans*, *120*, 942–957, doi:10.1002/2014JC010098.

Received 30 APR 2014
Accepted 5 JAN 2015
Accepted article online 9 JAN 2015
Published online 18 FEB 2015

Analysis of riverine suspended particulate matter fluxes (Gulf of Lion, Mediterranean Sea) using a synergy of ocean color observations with a 3-D hydrodynamic sediment transport model

Vincent Le Fouest[1], Malik Chami[1,2], and Romaric Verney[3]

[1]Laboratoire d'Océanographie de Villefranche, Université Pierre et Marie Curie and CNRS, Villefranche sur Mer, France, [2]Institut Universitaire de France, Paris, France, [3]Laboratoire de Physique Hydrodynamique et Sédimentaire, Centre Bretagne, Institut Français de Recherche pour l'Exploitation de la Mer, Plouzané, France

Abstract The export of riverine suspended particulate matter (SPM) in the coastal ocean has major implications for the biogeochemical cycles. In the Mediterranean Sea (France), the Rhone River inputs of SPM into the Gulf of Lion (GoL) are highly variable in time, which severely impedes the assessment of SPM fluxes. The objectives of this study are (i) to investigate the prediction of the land-to-ocean flux of SPM using the complementarity (i.e., synergy) between a hydrodynamic sediment transport model and satellite observations, and (ii) to analyze the spatial distribution of the SPM export. An original approach that combines the MARS-3D model with satellite ocean color data is proposed. Satellite-derived SPM and light penetration depth are used to initialize MARS-3D and to validate its predictions. A sensitivity analysis is performed to quantify the impact of riverine SPM size composition and settling rate on the horizontal export of SPM. The best agreement between the model and the satellite in terms of SPM spatial distribution and export is obtained for two conditions: (i) when the relative proportion of "heavy and fast" settling particles significantly increases relative to the "light and slow" ones, and (ii) when the settling rate of heavy and light SPM increases by fivefold. The synergy between MARS-3D and the satellite data improved the SPM flux predictions by 48% near the Rhone River mouth. Our results corroborate the importance of implementing satellite observations within initialization procedures of ocean models since data assimilation techniques may fail for river floods showing strong seasonal variability.

1. Introduction

Continental shelves represent only 8% of the global ocean surface area, but play an important role in the earth carbon cycle [*Borges*, 2005]. They sustain one fourth of the global ocean primary production primarily fueled by oceanic and riverine nutrients [*Smith and Hollibauch*, 1993]. About 80% of the organic carbon present in the water column will ultimately be buried and stored in the continental shelves [*Hedges and Keil*, 1995]. In the coastal ocean, major rivers are a substantial source of terrigenous matter [e.g., *Milliman*, 2001]. Annually, they bring to the sea 1 Gt Carbon [*Hedges et al*., 1997]. Part of this particulate organic carbon (POC) pool is adsorbed onto riverine suspended particulate matter (SPM); the ratio POC/SPM varies within the range 1–35% [*van der Zee and Chou*, 2005; *Doxaran et al*., 2012; *Lorthiois et al*., 2012]. Less than 5% of this POC reaches the deep ocean realm [*Meade*, 1996]. Riverine fluxes of carbon are particularly important for the biological productivity and carbon cycle of oligotrophic systems.

The discharge of freshwater from the Rhone River, in the North Western Mediterranean Sea, is about 54 km^3 yr^{-1} at the river mouth [*Ludwig et al*., 2009]. This is about two orders of magnitude lower than the discharge from the world's largest river, the Amazon [*Dai and Trenberth*, 2002]. Similarly, the sediment load from the Rhone is estimated to 21–56 Mt yr^{-1} while it reaches about 1150 Mt yr^{-1} for the Amazon [*Dunne et al*., 1998; *Ollivier et al*., 2010]. However, in the Mediterranean Sea, the Rhone River represents the main source of riverine freshwater before the Po River (48 km^3 yr^{-1}) [*Dai and Trenberth*, 2002] as well as in terms of SPM load (net flux of 7.3 and 6 Mt yr^{-1} for the Rhone and the Po rivers, respectively) [*Cozzi and Giani*, 2011; *Ollivier et al*., 2010]. Finally, the Rhone River is the main contributor of freshwater and SPM to the Gulf of Lion (GoL) [*Cauwet et al*., 1990; *Syvitski and Kettner*, 2007; *Ollivier et al*., 2010]. The ambient concentration of

SPM within the GoL (along the shelf break) is very low, less than a few milligrams per liter. *Dufois et al.* [2014] suggested that part of the riverine sediments settle in the Rhone River prodelta and could be resuspended through the action of storms and surface waves and thereafter potentially transported seaward. Nevertheless, the impact of such events is principally limited to shallow waters (<50 m) farther west than the river mouth and plume area. River flash floods constitute the primary source of SPM within the GoL on a yearly basis [*Ollivier et al.*, 2010]. Over the course of 1 year, more than 80% of the solid discharge occurs in less than 45 days, with a high seasonal and interannual variability. The very short-term (i.e., a few days) variability of the Rhone River discharge and particulate inputs represent a severe limitation in accurately assessing the fluxes of riverine SPM within the ocean based on in situ data only. Complementary approaches can be used for reducing uncertainties in the determination of SPM fluxes within the coastal ocean in such strongly variable environments. They imply hydrodynamic ocean models coupled to sedimentary modules which are able to describe the distribution of SPM at a wide range of spatial and temporal scales characterizing highly dynamic shelf seas such as the North Sea [*El Serafy et al.*, 2011; *Souza et al.*, 2007]. Satellite data assimilation is used in this region where tides, winds, and waves represent major constraints on the fine sediment annual dynamics, particularly in the vast shallow water areas. The North Sea contrasts with the GoL, which is less subject to ambient sediment inputs. Nevertheless, the assessment of their predictive ability requires observations. SPM concentrations derived from ocean color remote sensing data are of great interest since they offer a high coverage in space and time.

The objectives of this study are (i) to investigate the prediction of the land-to-ocean flux of SPM using short-term reinitialization of a hydrodynamic sediment transport model with satellite observations, and (ii) to analyze the spatial distribution of the export of SPM into the GoL, which is a coastal environment subject to very synoptic pulses of riverine inputs of freshwater and SPM. For those purposes, an original approach is proposed based on the synergy of a three-dimensional (3-D) hydrodynamic and sediment transport model with satellite ocean color data. Typically, series of successive images of SPM satellite-derived products are used to first constrain and then to validate the hydrodynamic model. The paper is organized as follows. First, the methodology is described. Second, the results are presented. In particular, a sensitivity analysis is performed to determine the influence of the size and settling rate of particles on the horizontal export of SPM. The benefit of our approach relative to a satellite data assimilation technique is discussed as well.

2. Material and Methods

2.1. Study Area

The drainage basin of the Rhone River (Northwestern Mediterranean Sea, France) is one of the largest of Europe. The river is 812 km long and divides ~60 km upstream of its mouth into two branches so-called the "Grand Rhone" and the "Petit Rhone." The Grand Rhone drains 90% of the annual freshwater discharge and 85% of the solid discharge [*Pont*, 1992]. The current study will thus principally focus on the Grand Rhone river plume within the GoL. As the Grand Rhone River supplies 90% of the terrigenous material into the GoL [*Durrieu de Madron et al.*, 2000, 2003], such a coastal region could be classified as a case 2 water type [*Morel and Prieur*, 1977] for which the radiometric water leaving radiance is mostly ascribed to the combination of phytoplankton particles, mineral SPM, detrital particulate matter, and dissolved colored organic matter (CDOM). The horizontal and vertical distribution of SPM is controlled primarily by winds, by the intensity of the North Mediterranean Current flowing westward along the continental slope, and by flood events [*Millot*, 1999]. The input of freshwater from the Rhone River induces a salinity stratification, where a fresher surface layer is separated from the deeper saline waters of the Mediterranean Sea. Figure 1 shows the map of the study area.

2.2. In Situ Measurements and Remotely Sensed Ocean Color Data

To obtain concentrations of SPM from remote sensing observations of ocean color, an empirical regional relationship between field measurements of SPM and above water reflectance (R_{rs}) was used. From spring to autumn 2010 and 2011, radiometric measurements and SPM concentrations were acquired in the GoL (in the area of the Grand Rhone River) at 87 stations during five cruise campaigns [*Lorthiois et al.*, 2012]. The cruise campaigns occurred at different periods of the year (March, April, and November) to study various regimes of flood of the Rhone River (i.e., spring flood event, autumn flood event, and intermediate outflow). For each cruise, inshore-offshore transects were carried out with the ship to investigate the variability of the

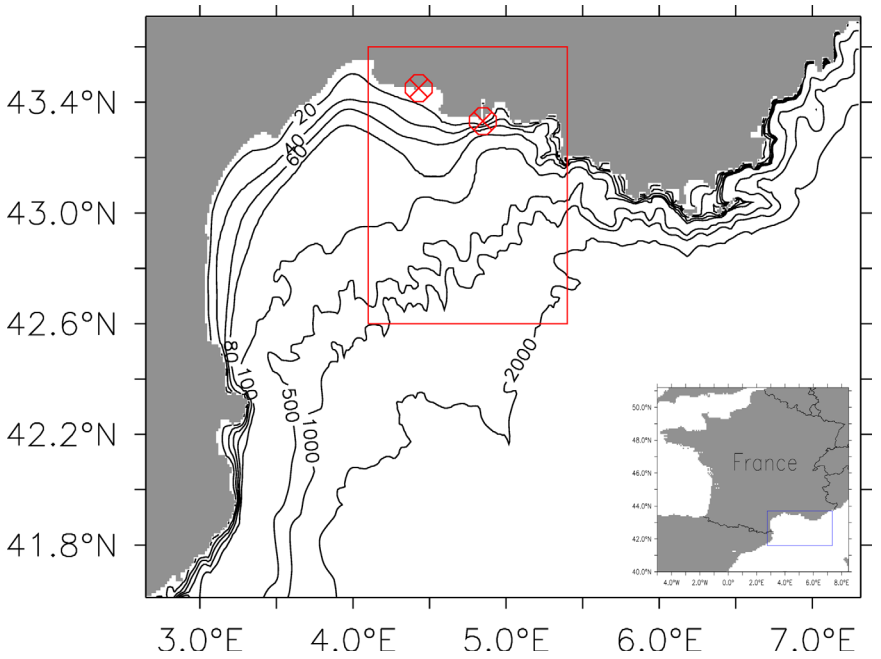

Figure 1. Bathymetry of the MARS-3D model grid in the Gulf of Lion (GoL). Red-crossed circles indicate the location of the "Petit Rhone" River (left-hand side) and the "Grand Rhone" River (right-hand side) inputs within the model. The red rectangle delimits the study area shown in Figures 6–10.

suspended matter in the study area. Concentrations of SPM were obtained by filtering 0.2–2 L of seawater, depending on turbidity, through precombusted (450°C) and preweighed 25 mm glass-fiber filters (Whatman, GF/F 0.7 μm nominal pore size). Note that the precombustion of the filters was performed before the cruise to ensure the use of clean filters during the field experiment. The filters were then dried for 24 h at 60°C and reweighed under a dry atmosphere to obtain the concentration of total suspended solids. The same seawater sample was filtered three times for a given station to get triplicates. The uncertainty in the measurements of the SPM concentration was determined as follows. The average and the standard deviation of the SPM concentration were calculated for each station. Then, the coefficient of variation (in %), which is defined as the ratio between the standard deviation and the average value, was determined for each station. Finally, the mean value of the coefficient of variation was calculated over all the stations to obtain the uncertainty in the overall measurements of SPM concentration, which was lower than 5% here [*Lorthiois*, 2012]. The SPM values varied within the range [1.40–39.0 g m^{-3}] over all the campaigns. The remote sensing reflectances, hereafter referred to as $R_{rs,}$ which are defined as the ratio between the upward radiance and the downwelling irradiance, were derived from measurements of upwelling radiance, sky radiance, and downwelling irradiance measured with a RAMSES stand alone and highly integrated hyperspectral radiance sensor (TriOS Company, Germany). Such a system of optical sensors measures above surface radiance and irradiance from UV to near infrared wavelengths (320–950 nm). Hyperspectral resolution of wavebands allows a spectral sampling increment of approximately 3 nm. The system consists of three optical sensors orientated to measure consecutively upwelling radiance, L_{usea}, sky radiance, L_{usky}, and downwelling irradiance, E_d. The downwelling irradiance sensor was set up at the top of the mast of the ship to avoid shadowing effects. The upward and downward radiance sensors were oriented at 45° from the nadir and vertical direction, respectively [see *Doxaran et al.*, 2006 for details].

Moderate Resolution Imaging Spectroradiometer (MODIS) satellite data at 500 m resolution were obtained from Goddard Distributed Active Archive Center (NASA) and processed in house using SeaDAS 6.4 data processing software. MODIS data were analyzed in consistency with the in situ measurements. The "MUMM Case 2 atmospheric correction" algorithm [*Ruddick et al.*, 2000] was used to process all MODIS data. The remotely sensed SPM concentration derived from MODIS observations (SPM_{MODIS}) was obtained using an empirical relationship adapted to the optically complex waters of the GoL:

$$SPM_{MODIS} = 670 \times \left(\frac{R_{rs}(555) \times R_{rs}(645)}{R_{rs}(469)} \right), \quad \text{RMSE} = 0.62 \text{ g SPM m}^{-3} \tag{1}$$

where $R_{rs}(555)$, $R_{rs}(645)$ and $R_{rs}(469)$ are the remotely sensed MODIS reflectances at 555, 645, and 469 nm, respectively. The multiband algorithm (equation (1)) generated SPM retrievals within 14% agreement from in situ concentrations. The coefficient of determination (R^2) between measured and remotely sensed SPM matchups was 0.82 and the Root Mean Square Error (RMSE) was 1.48 g SPM m^{-3} (Figure 2). The highest discrepancy occurred in the range (10–25 g SPM m^{-3}), which corresponds to intermediate values when dealing with the Grand Rhone river plume. The main limitation of our empirical algorithm is that its use could be questionable if the SPM concentration is higher than 40 g m^{-3}, which is the upper range of the field SPM data observed over all the cruises. This is because the reflectance signal at short wavelengths (469 and 555 nm) could saturate for greater SPM load, thus inducing a lower performance of the retrieval algorithm. Note, however, that *Forget et al*. [2001] reported that suspended solids at concentrations higher than 40 g m^{-3} are very rare off the Rhone River delta.

2.3. The Hydrodynamic Sediment Transport Model MARS-3D

A three-dimensional (3-D) ocean Model for Application at Regional Scale (so-called MARS-3D) [*Lazure and Dumas*, 2008] combined with a sedimentary module [*Verney et al*., 2013; *Dufois et al*., 2014] was used to simulate the spatial and temporal distribution of SPM within the study area. The ocean model used the incompressible, hydrostatic, and Boussinesq assumptions. The Navier-Stokes equations under the assumptions of Boussinesq and hydrostaticity [cf. *Lazure and Dumas*, 2008] were solved implicitly on an Arakawa type C grid [*Arakawa*, 1966] with a single time step of 10 s for both the baroclinic and barotropic mode. The model was eddy-permitting with a horizontal resolution of 1.2 km. Over the vertical layer, the model was discretized using a constant number of 30 levels (called "sigma levels") with the cell thickness varying according to the bathymetry. The free surface and bottom layer had a lower cell thickness to better resolve the processes at the interfaces. Bathymetry was derived from high-resolution (100 m) maps using depth measurements provided by the French Navy ("Service Hydrographique et Océanographique de la Marine (SHOM))" at the coast (from the shore line to 150 m depth) and from the U.S. National Geophysical Data Center (NGDC) 2 min global relief data set (so-called ETOPO2) [*NOAA*, 2001] for the offshore zone.

The MARS-3D model was constrained by atmospheric, oceanic, and hydrologic forcings. Atmospheric state (air temperature at 2 m height, surface winds at 10 m height, humidity, and downward long-wave and short-wave radiation) was taken from the three-hourly data sets of the atmospheric mesoscale model 5 (MM5) results. The MM5 is a regional mesoscale model used for creating weather forecasts and climate projections. The MM5 model is a limited area, nonhydrostatic, terrain-following sigma-coordinate model designed to simulate or predict mesoscale atmospheric circulation. It is a community model which was originally developed by the U.S. National Center for Atmospheric Research (NCAR) and the Pennsylvania State University (USA) [*Dudhia*, 1993; *Grell et al*., 1994]. Sponge layer boundary conditions prescribed at open boundaries for potential temperature, salinity, flow, and sea-surface elevation were provided from previous integrations of a regional configuration of the same model with a similar resolution (MENOR Configuration, [*André et al*., 2009, 2005]). Waves were simulated using the

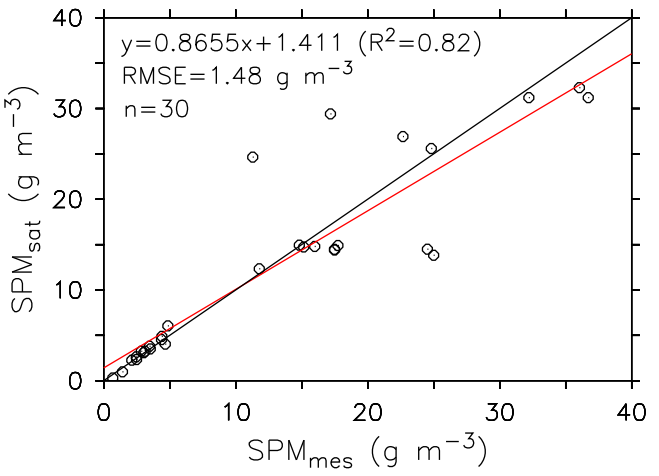

Figure 2. Scatter plot showing the linear relationship between measured SPM (SPM_{mes}, g m^{-3}) and satellite-derived SPM product (SPM_{sat}, g m^{-3}). The linear regression (in red) leads to the equation $SPM_{sat} = 0.86[SPM_{mes}] + 1.41$ with a coefficient of determination of $R^2 = 0.82$. The Root Mean Square Error (RMSE) is 1.48 g m^{-3}. The 1:1 line is in black.

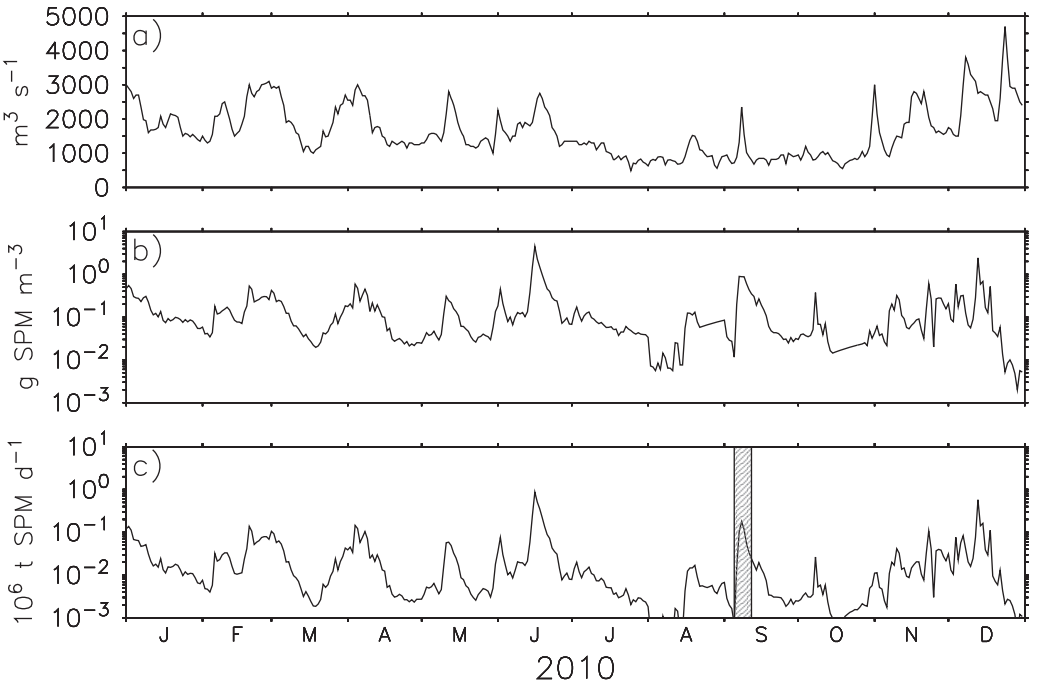

Figure 3. Seasonal inputs (from January to December 2010) measured in the Rhone River set as the riverine forcing in the MARS-3D model: (a) freshwater discharge ($m^3\ s^{-1}$), (b) total SPM concentration (SPM-L + SPM-H) ($g\ m^{-3}$), and (c) SPM riverine flux (i.e., the freshwater discharge multiplied by SPM concentration; 10^6 tons SPM d^{-1}). The shaded area (bottom) represents the time period analyzed in September 2010.

WAVEWATCH III® model (version 4.06) [*Ardhuin et al*., 2010; *Tolman*, 2008] implemented in the area on an unstructured mesh [*Ardhuin et al*., 2009; *Roland*, 2008]. This allowed the refinement of the mesh size close to the coast (∼100 m), where this information is the most relevant. Orbital velocities computed by WAVEWATCH III® at each node of the unstructured grid were interpolated to the Cartesian grid of the hydrodynamic model. As current velocities are weak in the area, no feedbacks are generated from the hydrodynamic model to the wave model. The wave model is forced at the open boundary by the regional wave model described in *Magne et al*. [2010] and forced by ECMWF (http://www.ecmwf.int/) operational wind analyses. The orbital velocity computed by the wave model from the full wave spectrum is used to calculate a wave shear stress, which is used to calculate the total wave-current shear stress [*Dufois et al*., 2014]. We neglect the effect of the wave/current relative direction by maximizing the total wave/current shear stress (angle = 0°), because the effect of the current is weak relative to the wave effect. A friction coefficient for waves of 0.06 and a bed roughness value of 0.0035 m for current-induced shear stress were used. The ocean model's hydrography was forced with fresh water flow measurements ($51.3 \times 10^9\ m^3\ yr^{-1}$) taken within the Rhone River at the Beaucaire station (43.92°N; 4.67°E) which is located 65 Km upstream from the river mouth (Figure 3a). With regard to the numerical grid, the main branch of the river, the Grand Rhone, is resolved over four grid cells while the Petit Rhone is resolved by one grid cell. The ability of the MARS-3D model to simulate the regional circulation and seawater properties within the GoL has been successfully assessed through comparisons with in situ and remotely sensed observations [*André et al*., 2009, 2005].

SPM concentrations measured inland near the city of Arles (France) at the Station Observatoire du Rhone à Arles (SORA) station were used as sediment inputs distributed at the river points (Figure 3b). The total riverine SPM input in the model (Figure 3c) was subdivided into "light and slow" settling fine sediments (hereafter referred to as SPM-L) and "heavy and fast" settling fine sediments (hereafter referred to as SPM-H). The scalars SPM-H and SPM-L are simulated explicitly in the model. Two fractions of particles (light and heavy particles) are tested because they are more realistic to represent the particulate river inputs to the ocean. The light particles (SPM-L) represent potentially large but very organic flocs which are found within the plume [*Dufois*, 2008], while the heavy particles (SPM-H) mimic dense flocs and/or very fine sands. This is a schematic view of sediment transport in the GoL to elaborate the values of settling velocities. Note that the settling velocities of SPM-L used in the model are consistent with those expected for the GoL (5×10^{-5}–8

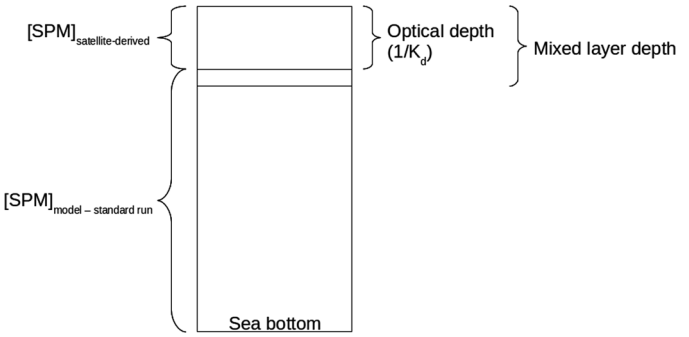

Figure 4. Schematic diagram depicting the initialization of the MARS-3D model using satellite-derived SPM data (see text for details).

$\times 10^{-4}$ m s^{-1}) [*Ulses et al*., 2008] (10^{-5}–10^{-4} m s^{-1}) [*Dufois*, 2008]. On this basis, a sensitivity analysis on the settling velocity model parameter is performed; such an analysis is detailed in next subsection 2.4.2. The range of settling velocities distinguishes between SPM-L [1.0×10^{-4} m s^{-1}–5.0×10^{-4} m s^{-1}] and SPM-H [2.0×10^{-4} m s^{-1}–1.0×10^{-3} m s^{-1}]. The settling velocity is computed in the model as a function of seawater turbulence and SPM concentration for SPM-L [*Dufois et al*., 2014], and as a function of SPM concentration only for SPM-H [*Verney et al*., 2013]. SPM settled throughout the water column to be ultimately stored into thin layers within the sediment compartment. The bed sediment can be eroded through the action of turbulence (both from currents and waves) and advection so that SPM can be transferred back to the water column using the Partheniades erosion law [*Verney et al*., 2013]. Bed sediment dynamics were intentionally downgraded, neglecting the sand fraction as the present work focuses on riverine slow settling fine sediment transfer in the vicinity of the Rhone river mouth and the associated turbid plume.

2.4. Synergy Approach Between MARS-3D and Satellite Observations

2.4.1. Initialization of MARS-3D Using Satellite Data

The MARS-3D model was initialized with near-equilibrium physical quantities (water level, 3-D horizontal velocities, salinity, and temperature) on 31 December 2009, but with no sediments in suspension. The model has a given spin-up period to initialize the physical circulation processes and the SPM conditions within the model. Here, the model was first run to simulate both the hydrodynamics and the SPM conditions during one full year, namely from 1 January 2010 to 31 December 2010. A 1 month spin-up period is used for suspended sediment (i.e., January 2010). Restart fields (both for hydrodynamics and sediments) are saved regularly and reused to focus on the key period studied in the present paper (e.g., a long time enough after initialization). The initialization procedure (Figure 4) follows two steps. First, for the date of interest (i.e., 5 September 2010), the SPM concentrations provided by the model were replaced by the satellite SPM measurements interpolated over the MARS-3D model grid. This approach that consists in using daily satellite observations of SPM to initialize the model is robust since the ambient SPM concentration is weak relative to the riverine flux at the GoL scale. Second, we used the light penetration depth ($1/K_d(490)$, in m) based on the satellite-derived diffuse attenuation coefficient in the visible part of the light spectrum ($K_d(490)$, in m^{-1}) to set the depth over which the remotely sensed SPM concentrations were assigned within MARS-3D. $K_d(490)$ was provided routinely by the MODIS data level 2 products. Note, however, that caution should be addressed to the use $K_d(490)$ since the wavelength of maximum solar penetration may be quite far removed from 490 nm for such optically complex waters. This approach prevents any arbitrary horizontal and vertical distribution of SPM within the model during the initialization phase. It is original in as much as it limits any possible vertical overestimation or underestimation of SPM within the turbid river plume and the ancillary clearer oceanic waters. The optical depth over which satellite SPM concentrations are used as inputs into the model is ~0–10 m within the plume. It is consistent with the upper mixed layer (UML) depth simulated by the model (<10 m, RMS = 6.1 m) and that reported in previous studies (1–8 m in average) [*Broche et al*., 1998; *Estournel et al*., 2001]. This implies that, in this study, there is no need for extrapolating the SPM satellite data to the sea bed since the ocean layer that could be observed by the satellite sensor (i.e., the light penetration depth) is consistent with the plume UML containing the most significant part of SPM. Because an extrapolation could be even more questionable when dealing with optically complex waters such as those found in the vicinity of river mouth, the use of the "standard run" of the MARS-3D model, which is defined later in section 2.4.2 as a run of reference with regard to the relative proportion of SPM-H versus SPM-L, was thus preferred to provide a value of SPM for the layers below. In other

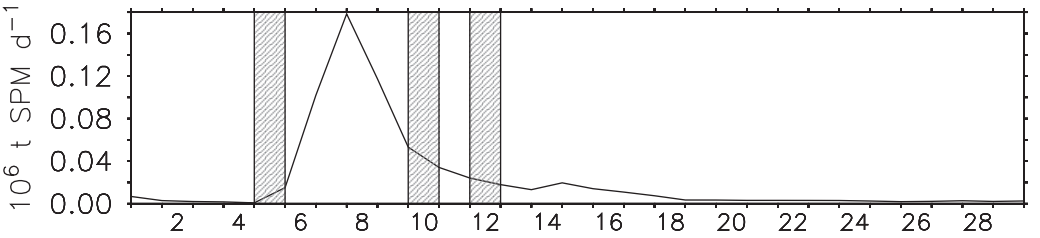

Figure 5. SPM flux (Mt SPM d^{-1}) measured in the Rhone River and set as the riverine forcing in the MARS-3D model in September 2010. The *x* axis represents the days of September 2010. The shaded areas represent the days for which MODIS estimates of SPM were available.

words, the model grid cells below the light penetration depth were assigned a value of SPM concentration derived from the MARS-3D standard reference run. This value was computed as an average SPM concentration for the vertical domain from the light penetration depth to the near-bottom depth of the model grid. Finally, the model predictions of SPM distribution will be later compared with satellite observations acquired several days after the initialization date (e.g., 10 September 2010) to assess the model performance.

In this study, an important flood event that occurred on 8 September 2010 was examined for three reasons. First, this flood event corresponded to a peak of freshwater flow (see Figure 3a). Second, it coincided with the third highest annual maximum of riverine SPM concentration and flux into the GoL (Figures 3b and 3c). Third, the simulated wave height was around 1 m and thus SPM resuspension contribution to the surface SPM in the prodelta region will be far lower than the riverine SPM contribution associated to the flood event. The pulsed nature of this event made it very relevant for assessing the fate of SPM exported into the GoL. Furthermore, clear satellite observations were available over the time period 5–12 September 2010 (Figure 5). The MARS-3D model was first initialized from "spun up" ocean conditions but with SPM derived from MODIS data 3 days before the flood event on 5 September (see Figure 5). MARS-3D model predictions of the distribution of SPM over the entire study area were then compared to satellite-derived SPM concentrations on 5, 10, and 12 September. The absolute values of SPM concentration and the absolute differences between the model and the satellite data were studied for 5, 10, and 12 September. In addition, the norm of the horizontal gradient of SPM concentration was examined as an informative metric on the predictive ability of the MARS-3D model.

2.4.2. Sensitivity Analysis Within MARS-3D

A sensitivity analysis was performed using MARS-3D to gain a better understanding of the physical processes driving the export and fate of riverine SPM. Our goal was also to improve the predictive ability of the MARS-3D model for simulating SPM concentrations and horizontal export fluxes. In a first step, the relative proportion of SPM-H versus SPM-L was modified within the Rhone River input. The so-called "standard run" was defined as a case for which SPM-L concentration contributes to 90% of the total mass of SPM relatively to SPM-H (10%) [e.g., *Bourrin et al*., 2008; *Pont*, 1992]. Such a case applies in the model to both low flow regime and high-flow periods. *Goineau et al*. [2012] estimated the proportion of heavy SPM (i.e., SPM-H) to 52% of the total mineral particles in December 2008 after a flood event (1450 m^3 s^{-1}). Based on this latter study, the model sensitivity was tested using an equal fraction of SPM-H and SPM-L (i.e., 50% each fraction).

Table 1. Summary of the Characteristics of the Runs Performed With MARS-3D Ocean Model[a]

			Standard Run	Run #2	Run #3	Run #4
SPM initialization with satellite data			No	Yes	Yes	Yes
Initialization dates				5 Sep 2010	5 Sep 2010	5 Sep 2010
SPM size fraction			90% SPM-L	90% SPM-L	50% SPM-L	50% SPM-L
			10% SPM-H	10% SPM-H	50% SPM-H	50% SPM-H
Settling rate (m s^{-1})	SPM-L	Min	$1\ 10^{-4}$	$1\ 10^{-4}$	$1\ 10^{-4}$	$5\ 10^{-4}$
		Max	$5\ 10^{-4}$	$5\ 10^{-4}$	$5\ 10^{-4}$	$10\ 10^{-4}$
	SPM-H	Min	$2\ 10^{-4}$	$2\ 10^{-4}$	$2\ 10^{-4}$	$10\ 10^{-4}$
		Max	$1\ 10^{-3}$	$1\ 10^{-3}$	$1\ 10^{-3}$	$5\ 10^{-3}$

[a]SPM notation stands for Suspended Particulate Matter, SPM-L stands for "light" suspended particulate matter and SPM-H stands for "heavy" suspended particulate matter.

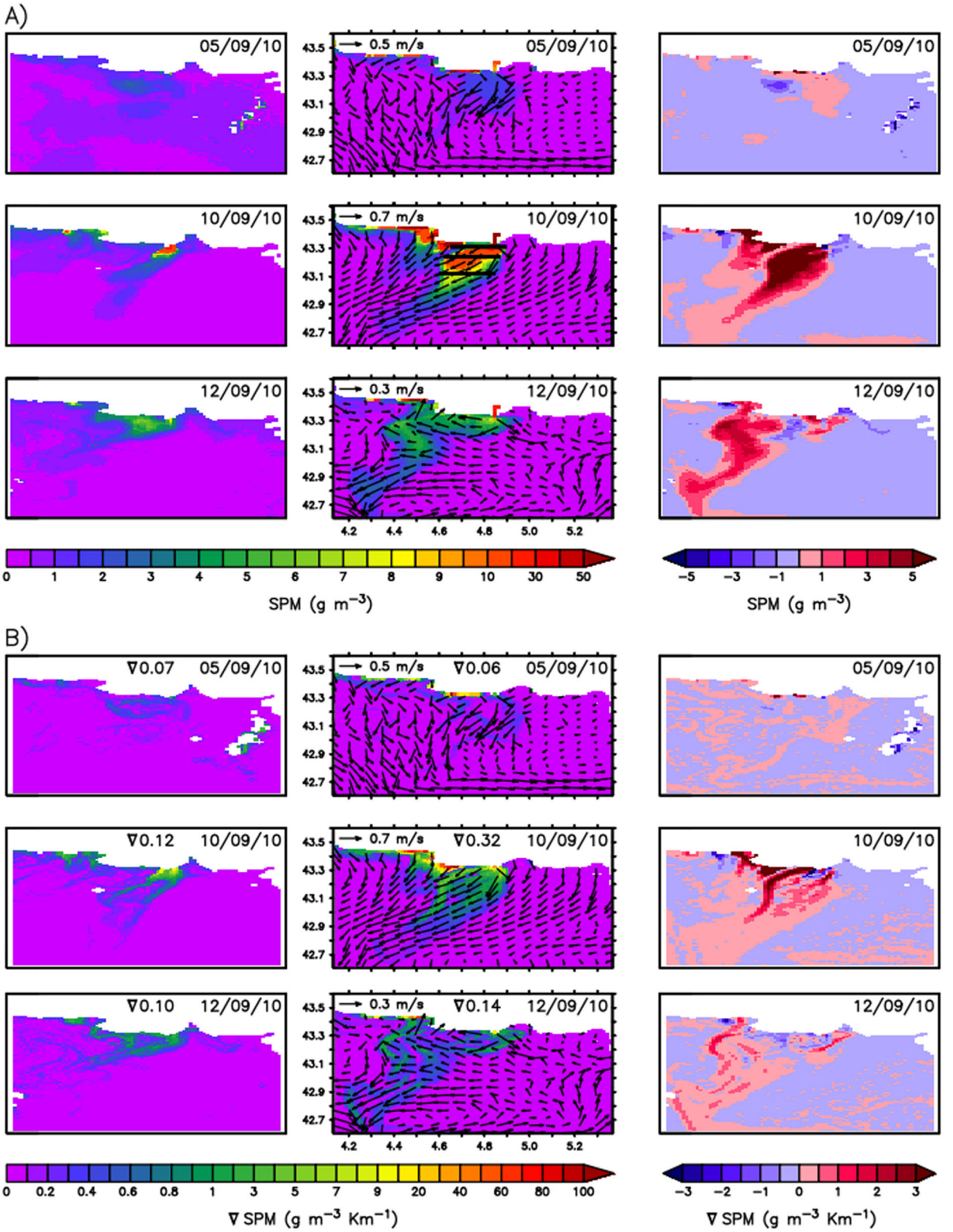

Figure 6. For the standard run of 5–10-12 September 2010: (a) satellite SPM concentration (g m^{-3}) (left plots), simulated surface SPM concentration (g m^{-3}), and surface currents (black arrows) (middle plots), and absolute difference (SPM_{model}-$SPM_{satellite}$, g m^{-3}) (right plots); (b) norm of the horizontal gradient of surface SPM concentration ($\nabla = \sqrt{\left(\frac{\partial SPM}{\partial x}\right)^2 + \left(\frac{\partial SPM}{\partial y}\right)^2}$; g m^{-3} km^{-1}, see equation (2)) derived from the satellite data (left plots), ∇_{mod}, g m^{-3} Km^{-1}) simulated by the model with surface currents (black arrows) (middle plots), and absolute difference ($\nabla_{mod} - \nabla_{sat}$, g m^{-3} km^{-1}) (right plots). In the top middle plot, the transects (bold black lines) used for the calculation of horizontal SPM fluxes (see Table 3) are shown. In Figure 6b, the average value of $\bigtriangledown$ (g SPM m^{-3} km^{-1}) over the entire surface area is mentioned at the top of each figure.

In a second step, because the range of variation of the SPM settling rates in coastal environments could be very wide (typically up to a fivefold factor) [see *Thill et al*., 2001], the minimum settling rate of both SPM-L (5.0×10^{-4} m s^{-1}) and SPM-H (1.0×10^{-3} m s^{-1}) was increased by a fivefold factor. All the run cases that were studied in the sensitivity analysis are described in detail in Table 1.

2.4.3. Horizontal Fluxes of Riverine SPM

Based on the simulated surface currents, the predicted and remotely sensed surface concentrations of SPM, horizontal fluxes of SPM were computed from the coast to the open ocean throughout transects 20 km long located within the river plume at 3.6, 32, and 64 km off the Grand Rhone River mouth (see Figure 6a). At each grid cell, the simulated or remotely sensed SPM concentration was multiplied by the north-south component of the currents simulated by the model to get fluxes. The flux was then integrated over the depth corresponding to the MODIS estimate of light penetration depth ($1/K_d$) over the transect length. This approach allows estimates of SPM fluxes based on the satellite data and their comparison with the MARS-3D model.

3. Results

Remote-sensing data show surface SPM concentrations on 5 September (before the flow peak) up to 1.5 g m^{-3} in waters less than 100 m deep and lower than 1 g m^{-3} in open and deeper waters (Figure 6a). Two days after the riverine peak of SPM (10 September), the river plume formed by the Grand Rhone outflow follows the 80 m isobaths (see Figure 1) and is oriented southwest. Its SPM signature extends offshore to depths greater than 500 m. SPM concentration values are up to 50 g m^{-3} in the vicinity of the river mouth and maintain high levels (10–50 g m^{-3}) in shallow waters (<70 m deep) up to 10 km off the coast. On 12 September, the plume is oriented mostly west-southwest and SPM concentrations decrease sharply. Concentrations of ~8 g m^{-3} are observed near the river mouth and concentrations within the range (3–6 g m^{-3}) are found up to 16 km offshore.

On 5 September, SPM concentrations are particularly overestimated along the coast (by up to 5 g m^{-3}) but show little differences with satellite data elsewhere (RMS = 0.86 g m^{-3}). Five days later on 10 September, i.e., 2 days after the peak of SPM flux, both the model and the satellite data agree on the river plume southwest orientation. However, the model markedly overestimates SPM concentrations within the plume, especially for concentrations within the range 4–50 g m^{-3}. Waters showing SPM concentrations greater than 10 g m^{-3} (red tones in Figure 6) extend up to 33 km offshore, which is more than 20 km further than concentrations observed in the satellite data (~11 km). The RMS error is the highest with a value of 3.64 g m^{-3}. A similar pattern is observed on 12 September with waters characterized by concentrations within the range 3–6 g m^{-3} spreading as a filament to 50 km off the coast, but with a lower RMS value (0.96 g m^{-3}) than the previous date.

To illustrate the dynamical coupling between the ocean currents and the SPM distribution in surface waters, the norm of the horizontal gradient of SPM (noted ∇ was computed between two grid cells in the model, or two pixels in satellite data, as follows:

$$\nabla = \sqrt{\left(\frac{\partial SPM}{\partial x}\right)^2 + \left(\frac{\partial SPM}{\partial y}\right)^2}, \tag{2}$$

where x and y are the grid axes in the east-west and north-south direction, respectively. At each grid cell, the centered derivatives were computed using a neighborhood of four locations adjacent to each cell (Rooks case contiguity) [see *Haining*, 2003]. This provides a measure of the horizontal gradient of surface SPM (horizontal dynamics) with respect to their settling rate from the shallow coastal waters to the deeper open waters (vertical dynamics). For instance, when ∇ has a value of 1 g SPM m^{-3} km^{-1}, this means that the SPM concentration decreases or increases by 1 g m^{-3} over 1 km. Figure 6b points out that the model satisfies fairly well the horizontal gradients depicted by the ocean color data. The differences between the model and the satellite data are greatest near the coast and within the plume but they are attenuated offshore. The average of ∇ over the study area was calculated (Figure 6b) to provide an insight into horizontal export of SPM. As ∇ increases, more SPM is exported horizontally toward the open ocean. Therefore, if more SPM are exported horizontally, this means that their vertical export with depth, given a location, is

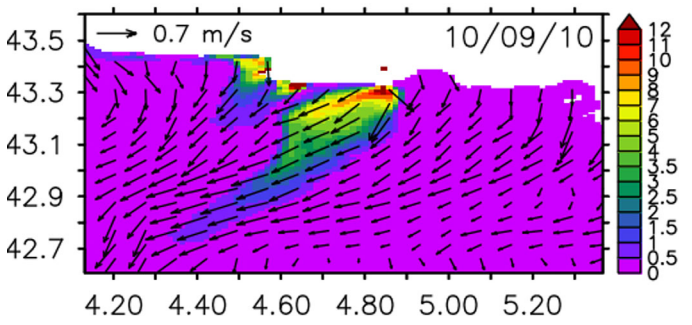

Figure 7. Simulated horizontal flux of surface SPM (g m^{-2} s^{-1}) computed from the standard run of the model for 10 September 2010.

necessarily reduced. Changes in ∇ could thus reflect indirectly changes in the vertical transport of SPM. The simulated horizontal flux, computed as the product of the norm of the velocity components and of the SPM concentration, was derived from the standard run of the model for 10 September (Figure 7). Figure 7 shows that the horizontal flux is oriented southward in the West direction with values decreasing from the coast to the open waters. It is interesting to highlight that the spatial patterns of the flux compare well with those of the gradient (Figure 6b, middle, 10 September 2010). In particular, it is observed that the norm of the gradient increases as the horizontal flux increases hence indicating that changes in the gradient reflect changes in the horizontal flux. The metric of the gradient defined in this study could thus be relevant to quantify somehow the horizontal export of the suspended matter. On 10 September, the area-averaged ∇ is 2.8-fold greater in the model (0.32 g SPM m^{-3} km^{-1}) than in satellite data (0.12 g SPM m^{-3} km^{-1}), suggesting that the simulated vertical export is likely underestimated. The high differences between the model and the satellite data in SPM concentration (Figure 6a) and in ∇ (Figure 6b) within the plume area are likely explained by the relative composition of the SPM pool (i.e., light versus heavy particles) in the Rhone River and/or by their settling velocity. To test these hypotheses, a sensitivity analysis dealing with these two parameters of the model (composition and settling rate of particles) was performed. The satellite-derived horizontal fields of K_d and SPM concentration were used for the initialization of MARS-3D (run 2, 3, and 4) (cf. section 2.4). The performance of the model runs relative to the satellite observations of SPM is evaluated using the area-averaged ∇ as a metric of comparison.

With regard to run 2 (i.e., SPM-L = 90% and SPM-H = 10%, initialization from satellite data), the simulated ∇ matches, as expected, with the standard run (∇ = 0.07 g SPM m^{-3} km^{-1}, Table 2) for the day when the model is initialized with satellite-derived SPM (5 September). On 10 September, the SPM concentration markedly decreases along the western coastline and farther offshore (Figure 8). The value of ∇ decreases by 37% (0.32–0.20 g SPM m^{-3} km^{-1}) with respect to the standard run hence reducing the bias with the satellite data (from +166 to +66%). Two days later, ∇ is 7% lower in run 2 (∇ = 0.13 g SPM m^{-3} km^{-1}) than in the standard run (∇ = 0.14 g SPM m^{-3} km^{-1}). However, the simulated ∇ remains 30% higher than that obtained directly from satellite observations. In terms of SPM concentration, the RMS error in run 2 is reduced by 64, 41, and 21% in 5, 10, and 12 September, respectively, relative to the satellite-derived data.

The model overestimation of SPM concentrations is significantly reduced in run 3 in which the contribution of SPM-L and SPM-H within the model grid are in equal proportion (i.e., 50%). On 10 September, 2 days after the peak of riverine SPM flux, the extent of surface waters with SPM concentrations within the range 10–50 g m^{-3} decreases to be in better agreement with the satellite data (Figure 9). The mean horizontal gradient (∇ = 0.13 g SPM m^{-3} km^{-1}, Table 2) is one-third lower than in run 2. Similarly, the RMS error decreased by 39% (2.13–1.3 g m^{-3}) relative to run 2.

Changes in SPM concentrations in the Petit Rhone discharge area are limited. Two days later, the surface area covered by waters having SPM in the range 3–6 g m^{-3} substantially decreases compared to run 2 and

Table 2. Surface Horizontal Gradient of SPM (in g m^{-3} km^{-1}) Averaged Over the Entire Study Area for the September Time Period[a]

September 2010	Satellite Data	Standard Run	Run 2	Run 3	Run 4
5th	0.07	0.06 (−14%)	0.07	0.07	0.07
10th	0.12	0.32 (+166%)	0.20 (+66%)	0.13 (+8%)	0.12
12th	0.10	0.14 (+40%)	0.13 (+30%)	0.07 (−30%)	0.08 (−20%)

[a]The percentage mentioned in brackets is the relative difference (in %) between the model runs and the satellite data.

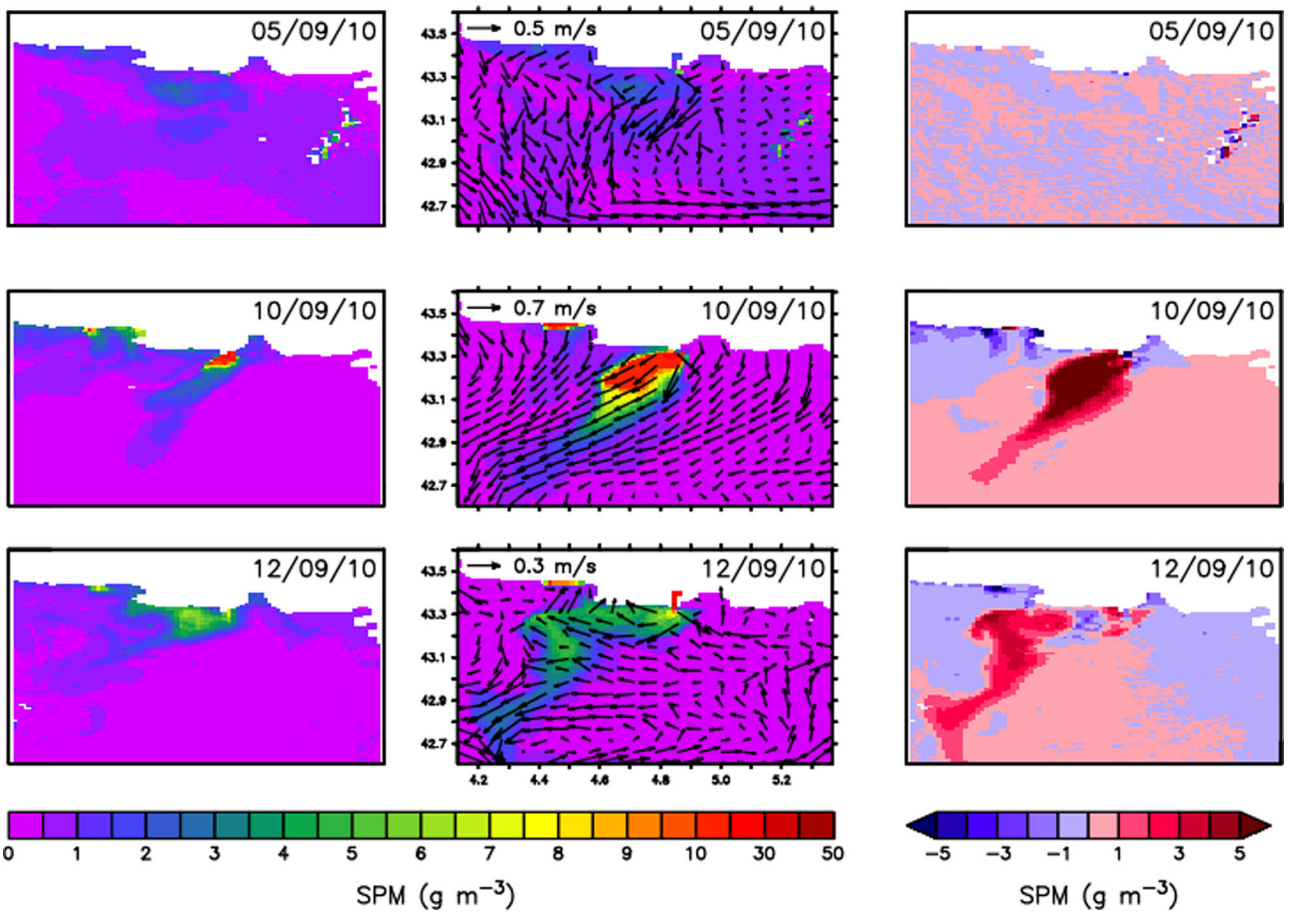

Figure 8. For run 2, satellite SPM concentration (g m^{-3}) (left plots), simulated surface SPM concentration (g m^{-3}) and surface currents (middle plots), and absolute difference (SPM_{model}-$SPM_{satellite}$, g m^{-3}) (right plots) for 5-10-12 September 2010.

is limited to a few kilometers from the Grand Rhone mouth. Their extent is lower than that observed in satellite data. The mean horizontal gradient ($\nabla = 0.07$ g SPM m^{-3} km^{-1}, difference with satellite data of -30%) is better retrieved than in the standard run ($\nabla = 0.14$ g SPM m^{-3} Km^{-1}, difference with satellite data of $+40\%$), but the absolute difference with satellite data is comparable with that obtained from run 2. In terms of SPM concentration, the RMS error in 12 September is also lower in run 2 (0.63 g m^{-3}) than in the standard run (0.96 g m^{-3}).

The increase by fivefold of the settling rate of both SPM size classes (run 4) leads on 10 September to a decrease of the east-west extent of the Grand Rhone plume with SPM concentration varying in the range 10–50 g m^{-3}. The best match with satellite data is then observed (Figure 10). Nevertheless, waters with concentrations varying in the range 3–8 g SPM m^{-3} still extend too far offshore. The mean horizontal gradient ($\nabla = 0.12$ g SPM m^{-3} km^{-1}, Table 2) is 8% lower than in run 3 and the same as the gradient derived from the satellite data ($\nabla = 0.12$ g SPM m^{-3} km^{-1}). The RMS error decreased by 4% relative to run 3. On 12 September, the RMS is same as in run 2, but the mean horizontal gradient ($\nabla = 0.08$ g SPM m^{-3} km^{-1}) and difference with satellite data (-20%) are the lowest of the four runs and show the best agreement with the satellite data.

In all runs, the agreement in the horizontal SPM flux between the model and the satellite data increases from the open waters to the coast (Table 3), suggesting that the processes which control the SPM removal from the surface to the deeper waters may be inappropriate in offshore waters for this case study. The SPM fluxes simulated in run 4 (i.e., initialization with satellite, SPM-L = 50% and SPM-H = 50%, fivefold increase of the settling rate of SPM-L and SPM-H) best compare with those estimated from the satellite data. At 3 km off the river mouth (transect 1), the relative difference between the model (0.069 Mt SPM d^{-1} in run 4; see

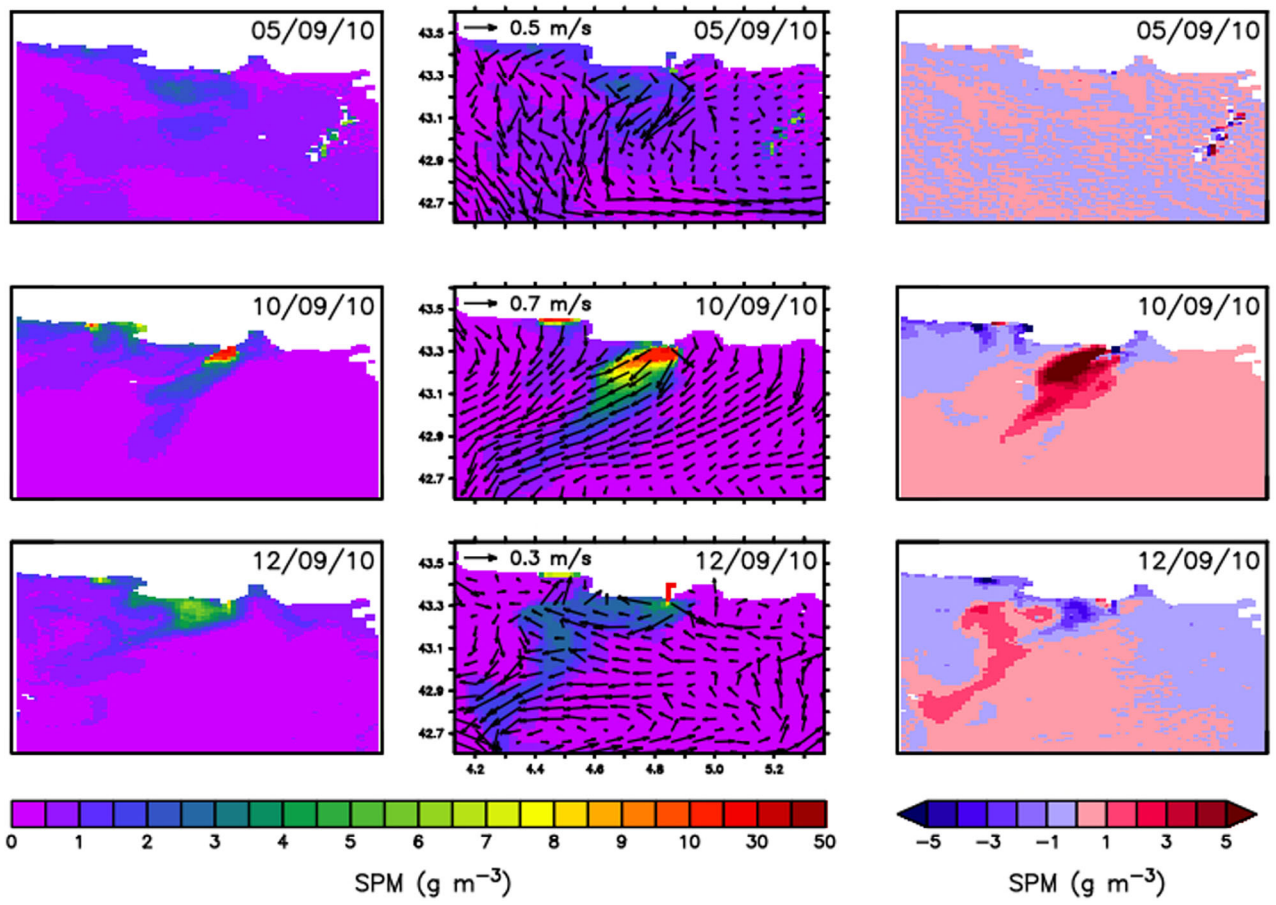

Figure 9. For run 3, satellite SPM concentration (g m^{-3}) (left plots), simulated surface SPM concentration (g m^{-3}) and surface currents (middle plots), and absolute difference (SPM_{model}-$SPM_{satellite}$, g m^{-3}) (right plots) for 5-10-12 September 2010.

Table 3) and the satellite flux estimates (0.035 Mt SPM d^{-1}) is the lowest (+97%) compared to the other 3 runs (+123 to +280%).

4. Discussion

The predictive ability of the regional hydrodynamic sediment transport model MARS-3D model is substantially improved when it is initialized using remotely sensed satellite estimates of SPM concentration and of the light penetration depth ($1/K_d$). In addition to using remotely sensed satellite SPM data to constrain the 3-D hydrodynamic sediment transport model, the main advantage of considering satellite observations of light penetration depth is to make more realistic the parameterization of the vertical distribution of SPM concentrations within the transport model. Another asset of using optical K_d data relies on the possibility to discriminate the river plume from the ancillary clearer waters. As an example, the recent study of *El Serafy et al*. [2011] does not take into account such optical property of the water column since it assumes that only the first vertical sigma layer of the 3-D hydrodynamic sediment transport model is equivalent to the light penetration depth observed. As underlined by these authors, such an assumption could have led to inconsistencies between the assimilated ocean color data and the model. Furthermore, close to the shoreline (<5 km), where the SPM concentrations were the highest, the first sigma level in our model is as low as a few centimeters. The model cell thickness was much lower than the MODIS-derived light penetration depth, which was around a few meters. *El Serafy et al*. [2011] pointed out that the use of remotely sensed light penetration depths could decrease the mismatch between the remotely sensed and simulated concentrations of SPM, which is consistent with our results. The successful synergy performed in this study between the model and the satellite data promotes the exploitation of 2-D synoptic products derived from

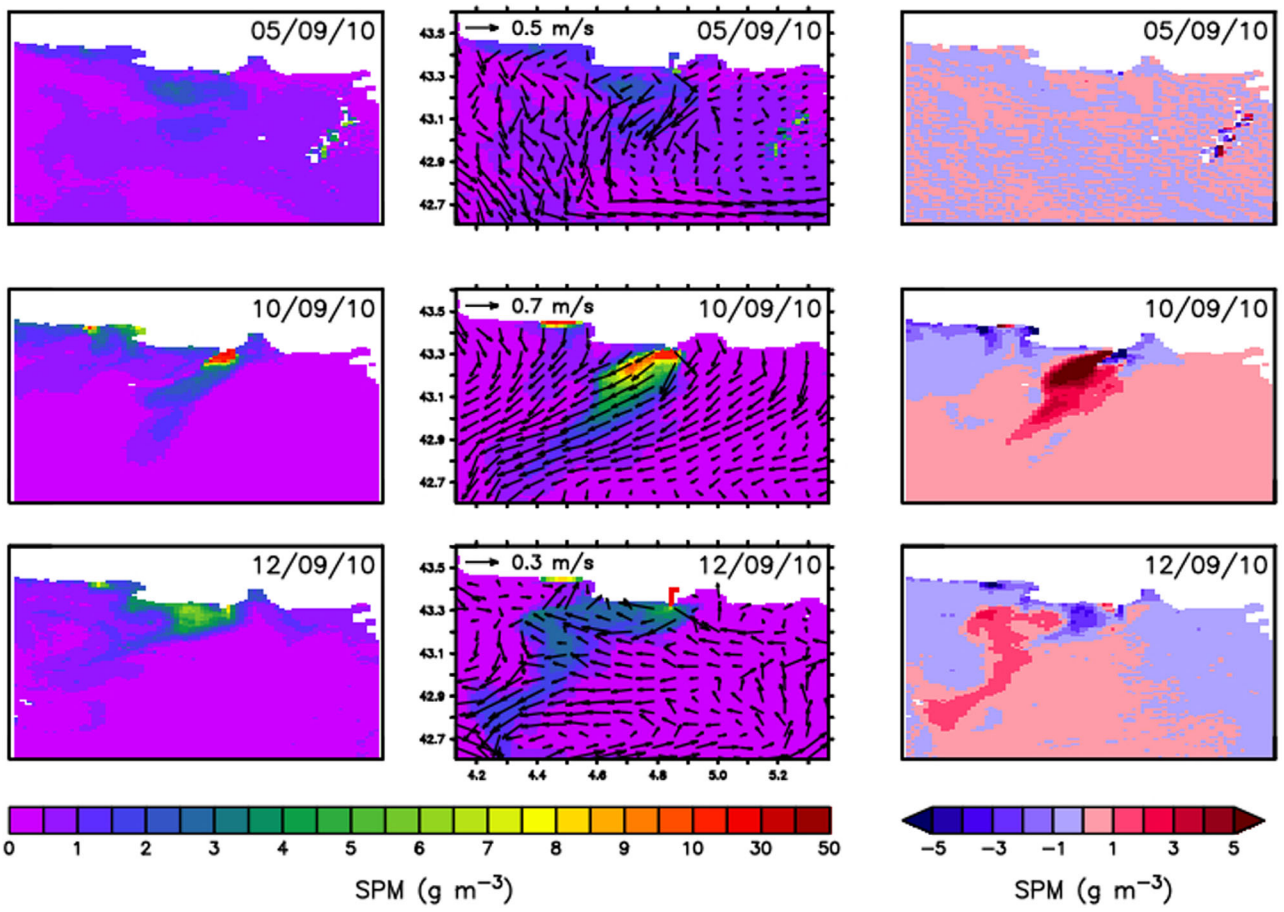

Figure 10. For run 4, satellite SPM concentration (g m^{-3}) (left plots), simulated surface SPM concentration (g m^{-3}) and surface currents (middle plots), and absolute difference (SPM_{model}-$SPM_{satellite}$, g m^{-3}) (right plots) for 5–10-12 September 2010.

ocean color data along with a 3-D hydrodynamic sediment transport model to better predict and analyze the horizontal (from the coast to the open ocean) and vertical (from the surface to the bottom) export of riverine SPM within the GoL.

The deterministic approach with remotely sensed data initialization was preferred here to data assimilation techniques to force the model and ultimately to compute fluxes of riverine SPM from the coast to the open ocean. This choice was principally motivated by the pulsed behavior of the Rhone River floods associated to the highly variable meteorological conditions along the drainage basin, which strongly constrain the riverine SPM inputs into the sea. The Northwestern Mediterranean Sea is a relatively cloud-free environment. In 2010, MODIS estimates of SPM concentration covered 50 days of 365 (13.7%). Nevertheless, only five satellite images were acquired within ±2 days of a peak in river discharge (two in April, one in June, one in September, and one in December) limiting, as a result, the efficiency of a data assimilation procedure. As a comparison, in their effort to improve the skills of a hydrodynamic sediment transport model for simulating SPM within the

Table 3. Southward Fluxes of SPM Across the Grand Rhone River Plume (Mt d^{-1}) on September 10 (Transect 1, 2, and 3 Are Located 3.6, 32, and 64 km From the Coast, Respectively)[a]

	Satellite Data	Standard Run	Run 2	Run 3	Run 4
Transect 1	0.035	0.133 (+280%)	0.128 (+266%)	0.078 (+123%)	0.069 (+97%)
Transect 2	0.017	0.117 (+588%)	0.109 (+541%)	0.067 (+294%)	0.067 (+294%)
Transect 3	0.011	0.053 (+382%)	0.054 (+391%)	0.032 (+191%)	0.032 (+191%)

[a]Fluxes were computed over the light penetration depth ($1/K_d$) derived from the MODIS data. The percentage mentioned in brackets is the difference between the model runs and the satellite data.

Southern North Sea, *El Serafy et al*. [2011] assimilated at least 30 MERIS images of SPM concentration to reduce the overall bias of the model by 10–14%. It is therefore not fully appropriate to use a data assimilation method in the GoL area due to the fact that strong seasonal variability of the freshwater Rhone River discharge events may not be overpassed by a sufficient number of satellite images for applying such methodology.

The benefit of using satellite data for the MARS-3D initialization step to improve the prediction of SPM fluxes near the river mouth (transect 1) could be easily quantified by calculating the relative difference between the case for which MARS-3D model is initialized using satellite data ("run 4" in Table 3) and the case for which MARS-3D is not initialized using satellite data ("standard run" in Table 3). Such a comparison points out a decrease of the flux estimates by −48% when satellite data are introduced into MARS-3D. In other words, this means that the synergy between satellite data and the MARS-3D model improves the prediction of SPM fluxes at the river mouth by 48%. Sensitivity analyses are hence required to determine the impact of riverine SPM size composition and settling rate on the SPM fluxes.

The annual input of SPM from the river set in the model (10.4 Mt) is in the midrange of the previously reported estimates (2–26.5 Mt) [*Ollivier et al*., 2010; *Pont et al*., 2002]. Those estimates being limited to the deltaic portion of the river, this study allows computing, for the first time to our knowledge, fluxes of surface SPM from the coast to the open ocean. Our sensitivity analysis showed that floods with a higher freshwater discharge are likely to be associated with a higher fraction of SPM-H entering the model (run 3) (see Figures 6 and 9). This result finds support in the study of *Antonelli and Provansal* [2002] that linked the amount of sand transported by the Grand Rhone with the flood type. For instance, more sand is exported during floods characterized by Mediterranean (i.e., rainfalls) and alpine (i.e., melting glaciers) SPM supplies. To that respect, the use of time invariant relative fractions of SPM-H and SPM-L to constrain the SPM inputs at the river points of the model appears inappropriate to compute land-to-ocean fluxes of SPM over the course of the year, which includes both low and high flood time periods. Further attention should be paid in the future to constrain the nature of the riverine SPM in hydrodynamic sediment transport models in a more accurate way for taking into account the significant seasonal variability of the fraction of suspended matter river inputs into the GoL.

As a perspective of the study, note that the export of SPM by rivers is tightly linked to the carbon cycle in the coastal ocean. The quantity of terrigenous POC drained to the coastal ocean and potentially buried in bottom sediments could be derived by predictive transport models based on SPM concentrations and on the ratio of POC over SPM (which could vary within the range 1–35%) [*van der Zee and Chou*, 2005; *Doxaran et al*., 2012; *Lorthiois et al*., 2012]. As the SPM concentration is more routinely monitored than POC in large rivers, accurate predictions of SPM concentrations and fluxes using regional hydrodynamic sediment transport models are a prerequisite to assess the fate of riverine POC into the coastal ocean. Furthermore, riverine SPM and POC are also optically active components that play a central role in the distribution of the underwater light field. However, their contribution to the transparency of river plume waters is poorly constrained in regional physical-biogeochemical models dedicated to the GoL study area [e.g., *Auger et al*., 2011]. As plumes often drain readily available nutrients for phytoplankton and bacterial growth, their effect on light attenuation in the water column should be accounted for to improve models predictions of biological production in coastal waters.

5. Conclusions

A 3-D hydrodynamic sediment transport model, namely MARS-3D, was initialized using MODIS satellite ocean color observations above the Gulf of Lion (Northwestern Mediterranean Sea, France). Horizontal 2-D fields of SPM satellite concentrations and light penetration depths ($1/K_d$) were obtained from a regional empirical remote sensing algorithm and from MODIS diffuse attenuation coefficients (K_d) data respectively. The originality of the approach which combines these two satellite-derived products of ocean color with an ocean model relies on the fact that vertical over- or underestimation of SPM within the turbid river plume and the ancillary clearer oceanic waters, respectively, is reduced through the use of satellite observations.

In line with effort promoted by the modeling scientific community [*Doney et al*., 2009; *Stow et al*., 2009], a quantitative metric was used to evaluate the MARS-3D model skills. This metric, namely the norm of the horizontal gradient of SPM, was calculated between two grid cells in the model or two pixels in satellite data to illustrate the dynamical coupling between the ocean currents and the SPM distribution in surface waters. The norm of the horizontal gradient of SPM is informative as well on the dispersion of surface SPM

with respect to their settling rate between the shallow coastal waters to the deeper open waters. Its use was particularly relevant in the study area which is characterized by a pronounced signature of the Grand Rhone River plume that contrasted with the clearer ancillary waters. Changes in the metric were hence tightly associated to changes in the SPM load within the plume.

The Rhone River input of SPM into the Gulf of Lion is characterized by pulsed export events. The consequence is a highly variable particulate size composition and settling rate depending on the river regime (low or high flood period). A sensitivity analysis was performed based on the initialization of MARS-3D with ocean color satellite data to evaluate the impact of riverine SPM size composition and settling rate on land-ocean fluxes of SPM predicted by the model. Results showed that the increase of the proportion of SPM-H relatively to SPM-L (from 10% SPM-H–90% SPM-L to 50% each) and the increase by fivefold of the settling rate of both size classes led to simulated distribution of SPM and exports in best agreement with the satellite SPM data (see Table 2). Therefore, particulate size and settling rate are key parameters during pulsed exports to gain understanding on the distribution of SPM. Our results also showed that the synergy between the MARS-3D model and the satellite ocean color data improved the land-ocean SPM fluxes model predictions by 48% in coastal waters near the river mouth. Such an improvement of MARS-3D prediction skills corroborates the need for implementing satellite observations within the initialization procedure of hydrodynamic ocean models that include a sedimentary module within the coastal ocean. Note that it was discussed as well that data assimilation techniques may not be fully appropriate in the study area due to the pulsed exports of the Rhone River over the course of the year. Future work could consist in investigating more intensively the seasonal variability of the SPM fluxes over the course of 1 year to better quantify the export of SPM into the coastal ocean and the biogeochemical implications in terms of carbon cycle. In this perspective, further work is required for a better characterization of the size composition of the riverine particulate inputs at the annual scale in the perspective of improving the performances of coastal ocean models predictions.

Acknowledgments

Vincent Le Fouest was supported by a research fellowship from the French space agency "Centre National d'Études Spatiales-CNES". The authors also wish to thank, by alphabetic order, David Doxaran, Bernard Gentili, Claire Neil, and Thomas Lorthiois from the Laboratoire d'Océanographie de Villefranche for having kindly provided in situ data and satellite image processing and Fabrice Ardhuin (IFREMER) for providing WW3 wave archive. IFREMER and NASA are gratefully acknowledged for having provided the MARS-3D model and the MODIS level 1 data. We are grateful to the reviewers for their relevant comments and suggestions which were helpful to improve the quality of the manuscript. The data for this study are available from the corresponding author at email address: vincent.le_fouest@univ-lr.fr.

References

André, G., P. Garreau, V. Garnier, and P. Fraunié (2005), Modelled variability of the sea surface circulation in the North-western Mediterranean Sea and in the Gulf of Lions, *Ocean Dyn.*, *55*, 294–308, doi:10.1007/s10236-005-0013-6.

André, G., P. Garreau, and P. Fraunié (2009), Mesoscale slope current variability in the Gulf of Lions. Interpretation of in-situ measurements using a three-dimensional model, *Cont. Shelf Res.*, *29*, 407–423, doi:10.1016/j.csr.2008.10.004.

Antonelli, C., and M. Provansal (2002), Characterisation and assessement of sand fluxes in the lower Rhone river, France, in *Proceedings of River Flow 2002*, vol. 1, pp. 587–593,A. A. Balkema, Louvain-la-Neuve, Belgique.

Arakawa, A. (1966), Computational design for long-term numerical integration of the equation of fluid motion: Two dimensional incompressional flow, part 1, *J. Comput. Phys.*, *1*, 119–143.

Ardhuin, F., L. Marié, N. Rascle, P. Forget, and A. Roland (2009), Observation and estimation of Lagrangian, Stokes, and Eulerian currents induced by wind and waves at the sea surface, *J. Phys. Oceanogr.*, *39*, 2820–2838, doi:10.1175/2009JPO4169.1.

Ardhuin, F., et al. (2010), Semi-empirical dissipation source functions for wind-wave models: Part I, definition, calibration and validation, *J. Phys. Oceanogr.*, *40*, 1917–1941.

Auger, P. A., F. Diaz, C. Ulses, C. Estournel, J. Neveux, F. Joux, M. Pujo-Pay, and J. J. Naudin (2011), Functioning of the planktonic ecosystem on the Gulf of Lions shelf (NW Mediterranean) during spring and its impact on the carbon deposition: A field data and 3-D modelling combined approach, *Biogeosciences*, *8*, 3231–3261.

Borges, A. V. (2005), Do we have enough pieces of the jigsaw to integrate CO_2 fluxes in the coastal ocean? *Estuaries*, *28*, 3–27.

Bourrin, F., P. L. Friend, C. L. Amos, E. Manca, C. Ulses, A. Palanques, X. Durrieu de Madron, and C. E. L. Thompson (2008), Sediment dispersal from a typical Mediterranean flood: The Tet River, Gulf of Lions, *Cont. Shelf Res.*, *28*, 1895−1910, doi:10.1016/j.csr.2008.06.005.

Broche, P., J. Devenon, P. Forget, J. de Maistre, J. Naudin, and G. Cauwet (1998), Experimental study of the Rhone plume. Part I: Physics and dynamics, *Oceanol. Acta*, *21*, 725–738.

Cauwet, G., F. Gadel, M. M. de Souza Sierra, O. Donard, and M. Ewald (1990), Contribution of Rhone River to organic carbon inputs to the northwestern Mediterranean Sea, *Cont. Shelf Res.*, *10*, 1025–1037.

Cozzi, S., and M. Giani (2011), River water and nutrient discharges in the Northern Adriatic Sea: Current importance and long term changes, *Cont. Shelf Res.*, *31*, 1881–1893, doi:10.1016/j.csr.2011.08.010.

Dai, A., and K. E. Trenberth (2002), Estimates of freshwater discharge from continents: Latitudinal and seasonal variations, *J. Hydrometeorol.*, *3*, 660–687.

Doney, S. C., I. Lima, J. K. Moore, K. Lindsay, M. J. Behrenfeld, T. K. Westberry, N. Mahowald, D. M. Glover, and T. Takahashi (2009), Skill metrics for confronting global upper ocean ecosystem-biogeochemistry models against field and remote sensing data, *J. Mar. Syst.*, *76*, 95–112, doi:10.1016/j.jmarsys.2008.05.015.

Doxaran, D., R. C. N. Cherukuru, and S. J. Lavender (2006), Inherent and apparent optical properties of turbid estuarine waters: Measurements, modelling and application to remote sensing, *Appl. Opt.*, *45*, 2310–2324.

Doxaran, D., J. Ehn, S. Bélanger, A. Matsuoka, S. Hooker, and M. Babin (2012), Optical characterization of suspended particles in the Mackenzie River plume (Canadian Arctic Ocean) and implications for ocean colour remote sensing, *Biogeosciences*, *9*, 3213–3229.

Dudhia, J. (1993), A nonhydrostatic version of the Penn State/NCAR mesoscale model: Validation tests and simulation of an Atlantic cyclone and cold front, *Mon. Weather Rev.*, *121*, 1493–1513.

Dufois, F. (2008), Modélisation du transport particulaire dans le Golfe du Lion en vue d'une application au devenir des traceurs radioactifs issus du Rhone, PhD thesis, Université du Sud Toulon-Var, Toulon, France. [Available at http://archimer.ifremer.fr/doc/00000/6308.]

Dufois, F., R. Verney, P. Le Hir, F. Dumas, and S. Charmasson (2014), Impact of winter storms on sediment erosion in the Rhone River prodelta and fate of sediment in the Gulf of Lions (North Western Mediterranean Sea), *Cont. Shelf Res.*, *72*, 57–72, doi:10.1016/j.csr.2013.11.004.

Dunne, T., L. A. K. Mertes, R. H. Meade, J. E. Richey, and B. R. Forsberg (1998), Exchanges of sediment between the flood plain and channel of the Amazon River in Brazil, *GSA Bull.*, *110*, 450–467.

Durrieu de Madron, X., A. Abassi, S. Heussner, A. Monaco, J. C. Aloisi, O. Radakovitch, P. Giresse, R. Buscail, and P. Kerherve (2000), Particulate matter and organic carbon budgets for the Gulf of Lions (NW Mediterranean), *Oceanol. Acta*, *23*, 717–730.

Durrieu de Madron, X., et al. (2003), Nutrients and carbon budgets for the Gulf of L ion during the Moogli cruises, *Oceanol. Acta*, *26*, 421–433.

El Serafy, G. Y., M. A. Eleveld, M. Blaas, T. van Kessel, S. G. Aguilar, and H. J. Van der Woerd (2011), Improving the description of the suspended particulate matter concentrations in the Southern North Sea through assimilating remotely sensed data, *Ocean Sci.*, *46*, 179–202, doi:10.1007/s12601-011-0015-x.

Estournel, C., P. Broche, P. Marsaleix, J. L. Devenon, F. Auclair, and R. Vehil (2001), The Rhone river plume in unsteady conditions: Numerical and experimental results, *Estuarine Coastal Shelf Sci.*, *53*, 25–38, doi:10.1006/ecss.2000.0685.

Forget, P., P. Broche, and J. J. Naudin (2001), Reflectance sensitivity to solid suspended sediment stratification in coastal water and inversion, *Remote Sens. Environ.*, *77*, 92–103.

Goineau, A., et al. (2012), Temporal variability of lived (stained) foraminiferal faunas in a river-dominated shelf: Faunal response to rapid changes of the river influence (Rhone prodelta, NW Mediterranean), *Biogeosciences*, *9*, 1367–1388, doi:10.5194/bg-9-1367-2012.

Grell, G. A., J. Dudhia, and D. R. Stauffer (1994), A description of the fifth-generation Penn State/NCAR mesoscale model (MM5), *NCAR Tech. Note, NCAR/TN- 398+STR*, p. 138, Natl. Cent. for Atmos. Res., Boulder, Colo., doi:10.5065/D60Z716B

Haining, R. P. (2003), *Spatial Data Analysis: Theory and Practice*, 432 p., Cambridge Univ. Press, Cambridge, U. K.

Hedges, J. I., and R. G. Keil (1995), Sedimentary organic matter preservation: An assessment and speculative synthesis, *Mar. Chem.*, *49*, 81–115, doi:10.1016/0304-4203(95)00008-F.

Hedges, J. I., R. G. Keil, and R. Benner (1997), What happens to terrestrial organic matter in the ocean?, *Org. Geochem.*, *27*, 195–212.

Lazure, P., and F. Dumas (2008), An external-internal mode coupling for a 3D hydrodynamical model for applications at regional scale (MARS), *Adv. Water Resour.*, *31*, 233–250.

Lorthiois, T. (2012), Dynamique des matières en suspension dans le panache du Rhône (Méditerrannée Occidentale) par télédétection spatiale «couleur de l'océan», PhD dissertation, 227 pp., Univ. Pierre et Marie Curie, Paris, France.

Lorthiois, T., D. Doxaran, and M. Chami (2012), Daily and seasonal dynamics of suspended particles in the Rhone River plume based on remote sensing an fields measurements, *Geo Mar. Lett.*, *32*, 89–101, doi:10.1007/s00367-012-0274-2.

Ludwig, W., E. Dumont, M. Meybeck, and S. Heussner (2009), River discharges of water and nutrients to the Mediterranean and Black Sea: Major drivers for ecosystem changes during past and future decades?, *Prog. Oceanogr.*, *80*, 199–217, doi:10.1016/j.pocean.2009.02.001.

Magne, R., F. Ardhuin, and A. Roland (2010), Prévisions et rejeux des états de mer du globe à la plage, *Eur. J. Environ. Civ. Eng.*, *14*, 149–162, doi:10.3166/EJECE.14.149–162.

Meade, R. H. (1996), River-sediment inputs to major deltas, in *Sea-Level Rise and Coastal Subsidence: Causes, Consequences and Strategies*, edited by J. D. Milliman and B. U. Haq, pp. 63–85, Kluwer Academic publishers, Dordrecht, Netherlands.

Milliman, J. D. (2001), River inputs, in *Encyclopedia of Ocean Sciences*, edited by J. H. Steele, S. A. Thorpe and K. K. Turekian, pp. 2419–2427, Academic, San Diego, Calif.

Millot, C. (1999), Circulation in the Western Mediterranean sea, *J. Mar. Syst.*, *20*, 423–442.

Morel, A., and L. Prieur (1977), Analysis of variation in ocean color, *Limnol. Oceanogr.*, *22*, 709–722.

National Oceanic and Atmospheric Administration (NOAA) (2001), *ETOPO2, Topographic and Bathymetric Surface of the Earth at 2 Min Resolution*, Natl. Geophys. Data Cent., Boulder, Colo.

Ollivier, P., B. Hamelin, and O. Radakovitch (2010), Seasonal variations of physical and chemical erosion: A three-year survey of the Rhone River (France), *Geochim. Cosmochim. Acta*, *74*, 907–927, doi:10.1016/j.gca.2009.10.037.

Pont, D. (1992), Caracterisation de la charge solide en suspension du Rhône au niveau du Palier d'Arles lors d'une crue d'importance moyenne, Rapport final du groupe de travail Apports en Méditerranée, 25 pp., Agence de l'eau Rhône-Méditerranée-Corse, Laboratoire de Biologie Animale et Ecologie, Ecologie des Systèmes Fluviaux, France.

Pont, D., J. P. Simonnet, and V. Walter (2002), Medium-term changes in suspended delivery to the ocean: Consequences of catchment heterogeneity and river management (Rhone River, France), *Estuarine Coastal Shelf Sci.*, *54*, 1–18.

Roland, A. (2008), Development of WWMII: Spectral wave modelling on unstructured meshes, PhD thesis, Technische Universitat Darmstadt, Institute of Hydraulics and Water Resources Engineering, Darmstadt, Germany.

Ruddick, K. G., F. Ovidio, and M. Rijkeboer (2000), Atmospheric correction of SeaWiFS imagery for turbid coastal and inland waters, *Appl. Opt.*, *39*, 897–912.

Smith, S. V., and J. T. Hollibauch (1993), Coastal metabolism and the oceanic organiccarbon balance, *Rev. Geophys.*, *31*, 75–89.

Souza, A. J., J. T. Holt, and R. Proctor (2007), Modelling SPM on the northwest European shelf seas, in *Coastal and Shelf Sediment Transport*, edited by P. Balson and M. Colins, *Geol. Soc. London, Spec. Publ*. vol. 274, pp. 147–158, doi:10.1144/GSL.SP.2007.274.01.14.

Stow, C. A., J. Jolliff, D. J. McGillicuddy Jr., S. C. Doney, J. I. Allen, M. A. M. Friedrichs, K. A. Rose, and P. Wallhead (2009), Skill assessment for coupled biological/physical models of marine systems, *J. Mar. Syst.*, *76*, 4–15, doi:10.1016/j.jmarsys.2008.03.011.

Syvitski, J. P. M., and A. J. Kettner (2007), On the flux of water and sediment into the Northern Adriatic Sea, *Cont. Shelf Res.*, *27*, 296–308, doi:10.1016/j.csr.2005.08.029.

Thill, A., S. Moustier, J.-M. Garnier, C. Estournel, J.-J. Naudin, and J.-Y. Bottero (2001), Evolution of particle size and concentration in the Rhone river mixing zone: Influence of salt flocculation, *Cont. Shelf Res.*, *21*, 2127–2140.

Tolman, H. L. (2008), A mosaic approach to wind wave modeling, *Ocean Modell.*, *25*, 35–47.

Ulses, C., C. Estournel, X. Durrieu de Madron, and A. Palanques (2008), Suspended sediment transport in the Gulf of Lions (NW Mediterranean): Impact of extreme storms and floods, *Cont. Shelf Res.*, *28*, 2048–2070, doi:10.1016/j.csr.2008.01.015.

van der Zee, P., and L. Chou (2005), Seasonal cycling of phosphorus in the Southern Bight of the North Sea, *Biogeosciences*, *2*, 27–42, doi:1726-4189/bg/2005-2-27.

Verney, R., C. Jany, B. Thouvenin, I. Pairaud, M. Vousdoukas, C. Pinazo, F. Ardhuin, and P. Cann (2013), Sediment transport in the bay of Marseille: Role of extreme events, Proceedings of Coastal Dynamics 2013, in *7th International Conference on Coastal Dynamics*, 24–28 June 2013, pp. 1811–1822, Arcachon, France. [Available at http://archimer.ifremer.fr/doc/00204/31515/.]